

ДИСТАНЦИОННОЕ ЗОНДИРОВАНИЕ АТМОСФЕРЫ, ГИДРОСФЕРЫ  
И ПОДСТИЛАЮЩЕЙ ПОВЕРХНОСТИ

## Consistency between backscatter lidar products and visibility range

Valentin Mitev<sup>1</sup>, Renaud Matthey<sup>2\*</sup>

<sup>1</sup>CSEM, Rue de l'Observatoire 58, CH-2000 Neuchâtel, Switzerland

<sup>2</sup>University of Neuchâtel, Dep. of Science, CH-2000 Neuchâtel, Switzerland

Поступила в редакцию 3.09.2010 г.

We present a consistency of the following values: the aerosol backscatter coefficient (ABC) and top of Atmospheric Boundary Layer (ABL), derived from backscatter lidar measurements from one side, and the visually determined Visibility Range (VR) from the other. The VR is determined towards long-range reference topographic targets in horizontal or slant path, while the lidar measurement is performed in vertical. The mean extinction coefficient along line-of-sights to reference topographic objects is calculated from the lidar derived backscatter coefficient with model aerosol extinction-to-backscatter ratio (EBR), when necessary, taking into account the ABL top. The mean extinction coefficient along the line-of-sight to the reference target is also determined from the VR via Koschmieder equation. The correlation coefficient between the two data sets is  $R^2 = 0.86$  for all data points and  $R^2 = 0.91$  when selecting out the points with possible VR systematic error at the farthest reference target.

*Keywords:* backscatter lidar, aerosol backscatter, extinction coefficient, visibility range, Koschmieder equation.

### Motivation and Objectives

A motivation for this study is the quality control of ABC derived with elastic backscatter lidars. In the lidar networks such control is carried by numerical exercises and lidar inter-comparisons campaigns [1, 2]. Although well established, such procedures suffer from limitations. The numerical tests address only the processing algorithm. The intercomparison campaigns are expensive since they require to move the tested lidars to a common site. I.e. there is no self-consistent method for ABC quality control during the backscatter lidar operation at the home site.

Another motivation is the importance of VR for air traffic at airports [3]. Although this problem is addressed by backscatter lidars since a long time [3], there are still open questions. As the measurements shall be at slant-path, eye-safety regulations apply. Eye-safe wavelength probing means that the VR value shall be re-evaluated for the visible wavelength range. One solution may be lidar measurements in direction in which the eye-safety requirements may be relaxed (e.g., vertical) or at some distance from the airports. In such case, it is necessary to demonstrate the consistency between the extinction in vertical direction and slant-path VR.

The above motivations determine the objective in this study: to demonstrate the consistency between the backscatter lidar determined extinction coefficients

and ABL top altitude, with the VR to reference targets (objects) at horizontal and slant path direction.

### Lidar and Site

The lidar measurements are performed in Neuchâtel, Switzerland, 47.002°N, 6.955°E, 487 m above sea level (asl). The backscatter lidar used in this study is based on an instrument, initially developed for airborne operation [4, 5]. Its adaptation for ground-based operation and respective results were already reported elsewhere [2, 6, 7]. The performances of the main lidar subsystems are summarized in Table 1.

Table 1  
Specifications of the micro-pulse backscatter lidar

Laser/Wavelength	Micro-pulse/532 nm
Average power	18–20 mW
Polarization	Linear
Beam divergence	0.25 mrad (full angle)
Pulse repetition rate	5–6 kHz
Telescope type/aperture	Kepler type/50 mm
Field of view	0.5 mrad (full angle)
Interference filter: FWHM/Transmission	0.12 nm/38%
Range of full lidar overlap	400 m
Detection Type/Detectors	Photon counting/PMTs
Range resolution and single measurement duration	30 m/6 s

\* Valentin Mitev (valentin.mitev@csem.ch); Renaud Matthey (renaud.matthey-de-lendroid@unine.ch).

The ABC is derived with the classical Fernald's inversion procedure [8, 9]. The values for the molecular

Table 2

Reference topographic objects

No	Object	Range	Altitude (asl)	Note
1	Opposite shore of lake Neuchâtel	8–12 km, by azimuth	~ 470 m	<a href="http://fr.wikipedia.org/wiki/Lac_de_Neuch%C3%A2tel">http://fr.wikipedia.org/wiki/Lac_de_Neuch%C3%A2tel</a>
2	Mt Vully	15–20 km, by azimuth	653 m	<a href="http://fr.wikipedia.org/wiki/Mont_Vully">http://fr.wikipedia.org/wiki/Mont_Vully</a>
3	Mt Stockhorn	55 km	2190 m	<a href="http://en.wikipedia.org/wiki/Stockhorn">http://en.wikipedia.org/wiki/Stockhorn</a>
4	Wildstrubel	75 km	3243 m	<a href="http://en.wikipedia.org/wiki/Wildstrubel">http://en.wikipedia.org/wiki/Wildstrubel</a>
5	Mt Jungfrau	95 km	4158 m	<a href="http://en.wikipedia.org/wiki/Jungfrau">http://en.wikipedia.org/wiki/Jungfrau</a>

backscatter coefficient are obtained from meteorological radiosounding at Payerne Aerological Observatory, situated 20 km from Neuchâtel. The reference aerosol and molecular EBR (lidar ratios) are respectively 50 [10] and  $8\pi/3$  [9].

The position of the lidar site provides lines-of-sights to several reference topographic objects in Swiss Plateau and the Alpine ridge, that is, at direction south from Neuchâtel. This gives the opportunity to estimate VR visually by distinguishing the respective reference target (object) from its background [3, 11]. Table 2 presents a list of the reference topographic targets (objects) selected for this study. In most of the cases, the visibility and the cloud presence were also documented camera images, courtesy the Cantonal Police of Neuchâtel.

The VR,  $R_V$ , and the mean total extinction coefficient  $\sigma_{mean}$  along the line-of-sight are linked via Koschmieder equation [3, 11]. This relation is valid for wavelengths around 550 nm, and hence also for the lidar wavelength

$$R_V = 3.912/\sigma_{mean}. \quad (1)$$

This study is performed along the following steps:

- Lidar measurements with integration time of 1 hour; visual evaluation of  $R_V$ .
- Determination of the ABL top by gradient method [12] and the profile of ABC profile [8, 9] from the lidar signal.
- Evaluation of the total extinction coefficients (molecular plus aerosol one) from the lidar determined ABC and molecular backscatter coefficients and the respective reference lidar ratios.
- Determination of average values for the total extinction coefficient in ABL ( $\sigma_{ABL}$ ) and lower free troposphere till 4000 m ( $\sigma_{Tropo}$ ).
- Evaluation of the mean extinction coefficient along the line of sight to the reference object. Here we assume horizontal homogeneity of the atmosphere. For objects below ABL top, we consider  $\sigma_{mean} = \sigma_{ABL}$ ; for objects above ABL top, we consider:

$$\sigma_{mean} = \frac{\sigma_{ABL}}{R_T} R_1 + \frac{\sigma_{Tropo}}{R_T} R_2. \quad (2)$$

In (2)  $R_T$  is the distance to the reference target (object),  $R_1$  and  $R_2$  are the parts of  $R_T$  below and above the lidar determined ABL top, where  $R_1 + R_2 = R_T$ .

## Results

A total of 44 daytime lidar measurements were selected for this study, where the selection criterion is the stable synoptic situations, justifying the horizontal homogeneity of the atmosphere. Figure 1 presents two examples from the data set, for 11 March 2007 and 20 February 2007: respectively the lidar obtained ABC and the calculated total extinction coefficients profiles, and images in south direction. As it is seen, high values of the ABC are obtained during March 11, a day with low visibility range as illustrated by the image. Note that only the opposite shore of the lake is visible, while none of the objects further. This is opposite for February 20, when high visibility occurs, allowing to see the Alps ridge, with lidar measurements showing ABC value lower by an order of magnitude.

The lidar determined  $\sigma_{mean}$  and visually determined  $R_V$  for the selected data set are presented in Fig. 2. In addition to the objects given in Table 2, it was possible to insert a point with  $R_V \sim 5$  km, corresponding to a case thee opposite shore of the lake was not seen, but a boat in the middle of it was, what allowed  $R_V$  determination. The solid line in Fig. 2 presents the Koschmieder equation.

In our opinion, the main error source in such approach is in the visual  $R_V$  estimation: a statistical error for all reference and a systematic underestimation of  $R_V$  for the most remote object. In Fig. 2 there is a group of five points with  $\sigma_{mean}$  below  $3 \cdot 10^{-4} \text{ m}^{-1}$ . These values are associated with  $R_V = 95$  km, determined from the farthest reference target. This group of  $\sigma_{mean}$  values fits better with Koschmieder equation if we assume  $R_V \sim 150$  km rather than 95 km. This is confirmed by linear regression between  $\sigma_{mean}$  obtained from the lidar measurements and  $\sigma_{mean}$  obtained from visibility range via Koschmieder equation. Assuming that  $R_V = 95$  km for  $\sigma_{mean}$  below  $3 \cdot 10^{-4} \text{ m}^{-1}$ , we obtain  $R^2 = 0.86$ . In case

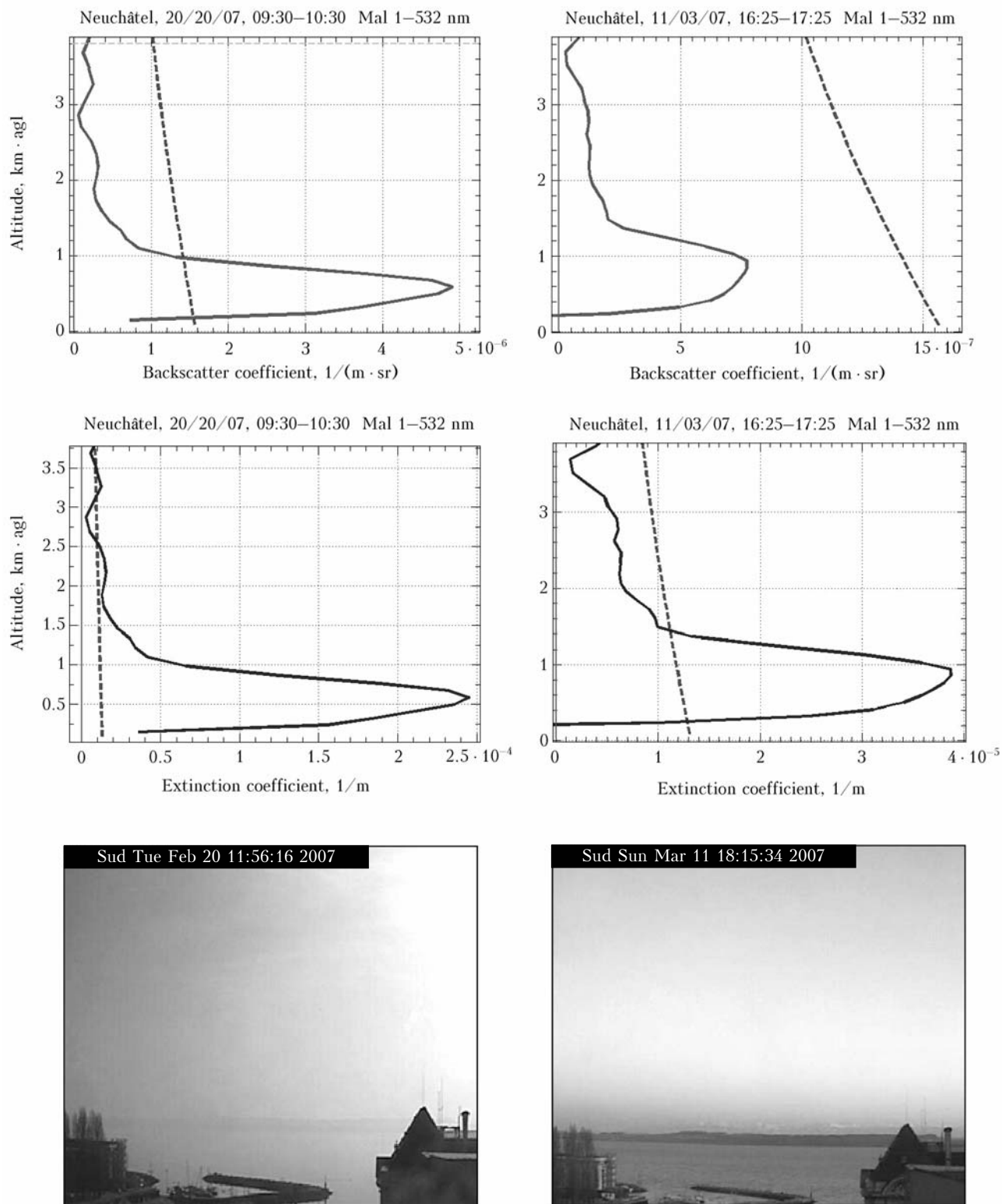


Fig. 1. Left column presents the case on 20 February 2007. Upper panel: solid – aerosol backscatter coefficient; dashed – molecular backscatter coefficient. Middle panel: solid – aerosol extinction coefficient; dashed – molecular extinction coefficient. Lower panel: A photo in direction Alps (South) taken during the measurement. The right column presents the same values and photo, but for 11 March 2007. The labels on the panels show the day and time in UTC

we assume  $R_V = 150$  km for  $\sigma_{mean}$  below  $3 \cdot 10^{-4} m^{-1}$ , we obtain  $R^2 = 0.91$ . The reason for under-estimation

is the fact that  $R_V$  could supersede 95 km, but a lack of farther references prevents such estimate.

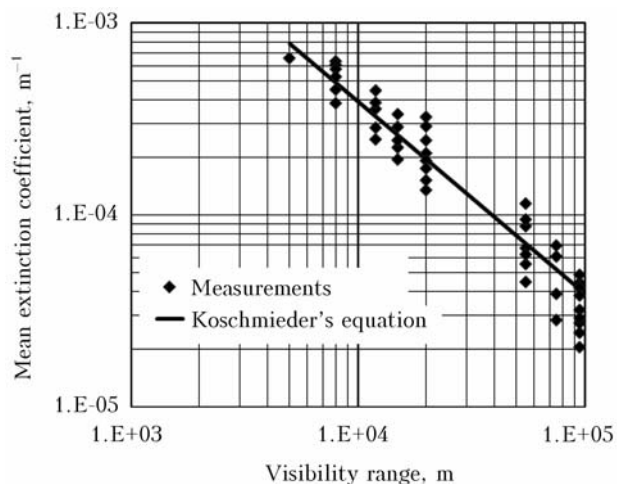


Fig. 2. Points are presenting the mean extinction as derived from the lidar measurements (vertical axis) and the estimated visibility range during the respective measurement (horizontal axis). The solid line shows Koschmieder's equation

## Conclusion

We presented dataset selected in stable atmospheric situations that demonstrates the consistency between the ABC and ABL top determined from backscatter lidar measurements from one side, and the visually determined VR from the other side. This consistency indicates to a possibility to use VR for quality control of the lidar determined ABC, with the advantage of availability at the lidar home site.

The demonstrated consistency also indicates that backscatter lidar measurements at vertical direction may provide monitoring of the slant path visibility at airports, in this way relaxing the eye-safety requirements. A subject of a further study will be to identify the number of points necessary for adequate VR evaluation.

## Acknowledgements

This work is performed in the frame of the EC project EARLINET-ASOS (RICA-025991). Gratitude is due to Payerne Aerological Station of Meteoswiss for the radiosonde profiles and to the Police of Neuchâtel for the camera images. The consultations in visibility range determination from Mme Joanna Baniewicz are greatly appreciated.

## References

- Christine Böckmann, Ulla Wandinger, Albert Ansmann, Jens Bösenberg, Vassilis Amiridis, Antonella Boselli,

- Arnaud Delaval, Ferdinando De Tomasi, Max Frioud, Ivan Videnov Grigorov, Arne Hegerd, Matej Horvat, Marco Iarlori, Leonce Komguem, Stephan Kreipl, Gilles Larchevêque, Volker Matthias, Alexandros Papayannis, Gelsomina Pappalardo, Francesc Rocadenbosch, Jose Antynio Rodrigues, Johannes Schneider, Valery Shcherbakov, and Matthias Wiegner, 2004: Aerosol Lidar Intercomparison in the Framework of the EARLINET Project. 2. Aerosol Backscatter Algorithms, *Appl. Opt.*, **43**, No. 4, pp. 977–989.
- Volker Matthias, Volker Freudenthaler, Aldo Amodeo, Ioan Balin, Dimitris Balis, Jens Bösenberg, Anatoly Chaikovskiy, Georgios Chourdakis, Adolfo Comeron, Arnaud Delaval, Ferdinando De Tomasi, Ronald Eixmann, Arne Hegerd, Leonce Komguem, Stephan Kreipl, Renaud Matthey, Vincenzo Rizi, José Antynio Rodrigues, Ulla Wandinger, and Xuan Wang, 2004: Aerosol Lidar Intercomparison in the Framework of the EARLINET Project. 1. Instruments, *Appl. Opt.*, **43**, No. 4, pp. 961–976.
- Christian Werner, Jürgen Streicher, Ines Leike and Christoph Münkel, *Visibility and Cloud Lidar // Lidar, Range-Resolved Optical Remote Sensing of the Atmosphere*, Claus Weitkamp (Editor), NY, Springer, 2005; pp. 165–186.
- Mitev V., Matthey R., Makarov V., 2002: Miniature backscatter lidar for cloud and aerosol observation from high altitude aircraft, *Recent Res. Devel. Geophysics*, ISBN:81-7736-076-0, Research Signpost. **4**, pp. 207–223.
- Corti T., Luo B.P., M. de Reus, Brunner D., Cairo F., Mahoney M.J., Martucci G., Matthey R., Mitev V., dos Santos F.H., Schiller C., Shur G., Sitnikov N.M., Spelten N., Vössing H.J., Borrmann S., and Peter T., 2008: Unprecedented evidence for overshooting convection hydrating the tropical stratosphere, *Geophys. Res. Lett.*, **35**, L10810, doi: 10.1029/2008GL033641.
- Giovanni Martucci, Renaud Matthey, Valentin Mitev, Two case studies of daily cycle PBL-dynamics over Basel; Backscatter lidar measurements, 22<sup>nd</sup> International Laser radar Conference (ILRC 2004), 1–16 July 2004, Matera, Italy, ESA SP-561 June 2004. Proceedings Vol. 2, pp. 765–768.
- Mitev V., Matthey R., Makarov V., 2010: Compact Micro-pulse Backscatter Lidar and examples of Measurements in the Planetary Boundary Layer, *Rumanian Journal of Physics* (in print).
- Fernald F.G., 1984: Analysis of atmosphere lidar observations: some comments, *Appl. Opt.*, **23**, pp. 652–653.
- Klett J.D., 1985: Lidar inversion with variable backscattering to extinction ratios, *Appl. Opt.*, **24**, pp. 1638–1643.
- Ackermann J., 1998: The Extinction-to-Backscatter Ratio of Tropospheric Aerosol: A Numerical Study, *J. Atmos. and Ocean. Technology*, **15**, pp. 1043–1050.
- Chu R., 1994: *Algorithms for the Automated Surface Observing System (ASOS)*, SL Office Note 94–4; NWS/OSD: Silver Spring, MD; p. 106.
- Martucci G., Matthey R., Mitev V., and Richner H., 2007: Comparison between Backscatter Lidar and Radiosonde Measurements of the Diurnal and Nocturnal Stratification in the Lower Troposphere, *J. Atmos. and Ocean. Technology*, **24**, pp. 1231–1244.